Polymer Journal (2022) 54:1119–1126
https://doi.org/10.1038/s41428-022-00661-9

ORIGINAL ARTICLE

Bioinspired macromolecular templates for crystallographic orientation control of ZnO thin films through zinc hydroxide carbonate

Takahiro Mikami[1] · Shunichi Matsumura[1] · Rino Ichikawa[1] · Riki Kato[1] · Junya Uchida[1] · Tatsuya Nishimura[1,3] · Takashi Kato[1,2]

Received: 10 March 2022 / Revised: 23 April 2022 / Accepted: 25 April 2022 / Published online: 10 June 2022

Abstract

The biomineralization-inspired preparation of inorganic hybrid materials has attracted attention. Here, we report a new approach to the orientation control of zinc oxide (ZnO) thin-film crystals through the preparation of zinc hydroxide carbonate (ZHC) by the macromolecular templates of poly(2-hydroxyethyl methacrylate) (PHEMA) and poly(vinyl alcohol) (PVA). Using 100-nm-thick PHEMA templates, ZHC thin films with the *c*-axis oriented parallel to the substrate were obtained, while ZHC thin films prepared by 100-nm-thick PVA templates showed perpendicular orientation. After the thermal treatment of ZHC, the crystal orientations of the ZnO thin films were maintained. The effects of the thickness and annealing time for the polymer templates on the morphologies of the ZnO thin films were examined.

Introduction

In nature, biological minerals are widely produced inside the tissues of organisms [1–8]. The crystallization of those biominerals is precisely controlled by bioorganic molecules, which results in the elaborate functional structures of biominerals. The morphologies and orientation of the inorganic crystals are beautifully engineered in ambient conditions [1–12]. Therefore, biominerals provide us with clues to establishing new environmentally friendly methods of developing inorganic materials with ordered structures [1–8]. Inspired by such biological crystallization mechanisms, macromolecular template approaches for $CaCO_3$ and hydroxyapatite (HAP; $Ca_{10}(PO_4)_6(OH)_2$) thin-film crystallization with various polymorphs, morphologies, and orientation were reported [3, 13–23]. Chitin [13, 14], chitosan [13, 14], cellulose [14, 15], poly(vinyl alcohol) (PVA) [16–21], poly(2-hydroxyethyl methacrylate) (PHEMA) [22], and poly(*N*-isopropyl acrylamide) [23] were used for the formation of thin-film crystals in insoluble polymer matrices as crystallization templates in collaboration with acidic, water-soluble polymers such as poly(acrylic acid) (PAA) and acidic peptides [24, 25].

On the other hand, it has been recognized that amorphous minerals play a key role in the formation of biominerals in nature [6, 26, 27]. In the synthetic system, amorphous $CaCO_3$ colloids can be stabilized by polymer additives [28–32]. These amorphous colloids serve as a precursor for spontaneous $CaCO_3$ crystallization in polymer matrices in aqueous solutions, which is similar to the biomineralization phenomena that occur in nature [29, 30, 33, 34].

Our intention here is to tune the crystallographic orientation for zinc hydroxide carbonate (ZHC) and zinc oxide (ZnO) thin films through the biomimetic macromolecular template approach (Fig. 1). Because ZnO has versatile

These authors contributed equally: Takahiro Mikami, Shunichi Matsumura

Supplementary information The online version contains supplementary material available at https://doi.org/10.1038/s41428-022-00661-9.

✉ Takashi Kato
kato@chiral.t.u-tokyo.ac.jp

[1] Department of Chemistry and Biotechnology, School of Engineering, The University of Tokyo, Bunkyo-ku, Tokyo 113-8656, Japan

[2] Research Initiative for Supra-Materials, Shinshu University, Wakasato, Nagano 380-8553, Japan

[3] Present address: Graduate School of Natural Science and Technology, Kanazawa University, Kakuma-machi, Kanazawa 920-1192, Japan

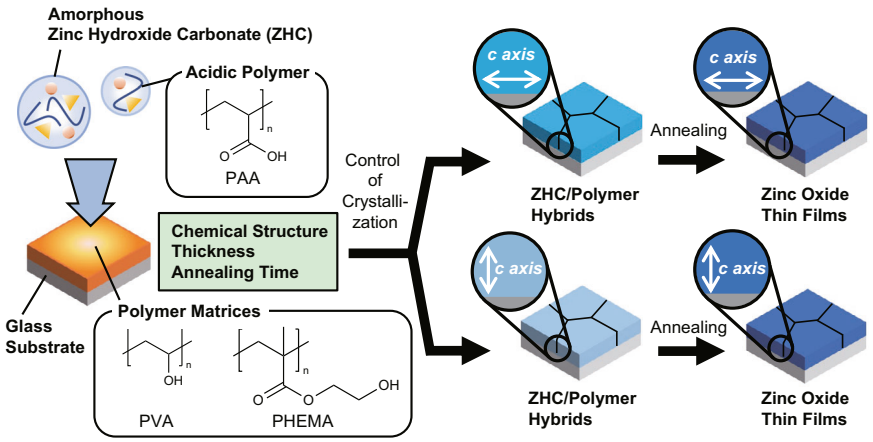

Fig. 1 Schematic illustration of the oriented ZnO thin-film synthesis strategy in this study through the biomimetic macromolecular template approach

applications in various electro-optic fields, the crystallization control of ZnO has been widely studied [35–40]. In particular, the aqueous-solution-mediated approach attracts much attention as a new way of manufacturing for a sustainable society. Biomineralization-inspired synthetic approaches are attractive because of their simple processes and low energy consumption. Previously, we reported the biomineralization-inspired preparation of ZHC and zinc hydroxide thin-film hybrids, which were converted to ZnO [41–43]. In this method, the polymer-stabilized amorphous precursors presumably infiltrate into the polymer matrix and induce crystallization. A ZnO thin film with the *c*-axis aligned perpendicular to the substrate was obtained by using PVA matrices [41]. In general, ZnO thin films are fabricated by widely used deposition methods, such as sputtering, chemical vapor deposition, and pulse vapor deposition. For these ZnO thin films, the *c*-axis of ZnO exhibited perpendicular alignment to the substrate [40]. There have been few reports on the synthetic methods of ZnO thin films with the *c*-axis aligned parallel to the substrate [44–46].

Here, we report a new macromolecular template method for the control of perpendicular and parallel orientations of thin-film crystals of ZHC and ZnO based on the PHEMA and PVA templates. To understand the template effects, we also fabricated ZnO thin films by varying the thickness and annealing time of the polymer matrices.

Experimental section

Materials

PHEMA ($M_v = 3.0 \times 10^5$), PVA ($M_w = 1.46$–1.86×10^5, 87–89% hydrolyzed), and PAA ($M_w = 1.8 \times 10^3$) were purchased from Sigma–Aldrich Japan (Tokyo, Japan). Zinc nitrate hexahydrate and ammonium carbonate were purchased from FUJIFILM Wako Pure Chemical (Osaka, Japan). All reagents were used without further purification.

Preparation of zinc hydroxide carbonate and zinc oxide thin films

To prepare the polymer matrix, PHEMA and PVA solutions in dimethylsulfoxide were spin-coated on glass substrates. After the matrix was annealed at 200 °C for 10 min, it was immersed in the solution prepared by mixing zinc nitrate hexahydrate aqueous solution containing PAA and ammonium carbonate aqueous solution. The final concentration of zinc nitrate hexahydrate and ammonium carbonate was 20 mM, and that of PAA was adjusted to 7.2×10^{-2} wt%. The PVA matrices were immersed in 4 ml of the solution for 24 h at 40 °C. After the crystallization processes, the samples were rinsed with purified water and dried in air. The resultant samples were annealed at 500 °C for 2 h.

Characterization

The morphologies of the samples were observed with scanning electron microscopy (SEM) (JSM-7800F Prime, operated at 3.0 kV, JEOL, Tokyo, Japan). SEM observations were performed with osmium coating. The crystal structures of the hybrids were analyzed by X-ray diffraction (XRD) (Smartlab, Rigaku, Tokyo, Japan) measurements using a parallel beam method with CuKα radiation (λ = 0.154 nm). To examine the crystallographic orientation, XRD measurements of the thin-film samples were recorded in two different geometries (i.e., out-of-plane with 2θ scanning and in-plane with $2\theta\chi$ scanning). The scanning directions of the out-of-plane and in-plane are perpendicular to the substrate and parallel to the substrate, respectively (Supplementary Fig. S1). The samples collected from the glass substrates were observed with transmission electron microscopy (TEM) (JEM-2000EX, operated at 200 kV, JEOL, Tokyo, Japan). The surfaces of the samples were observed with atomic force microscopy (AFM) (Multimode8, Bruker Japan K.K., Kanagawa, Japan) in the air at room temperature. Thermogravimetric measurements

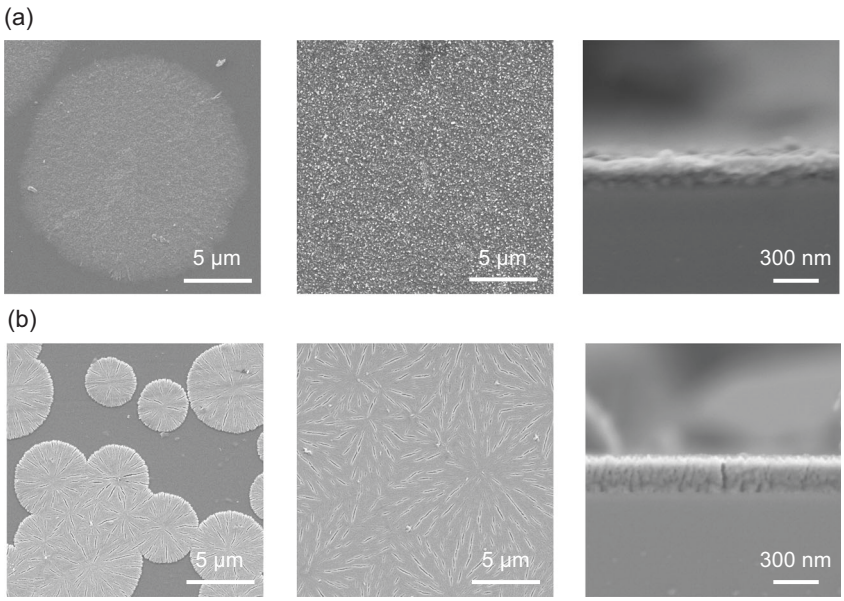

Fig. 2 **a** ZHC/PHEMA thin-film hybrids and **b** ZHC/PVA thin-film hybrids. SEM images of top-view surfaces of the spherulitic thin-film crystals grown in (left) 6 h, (middle) 24 h, and (right) cross-sectional SEM images of the hybrids

(TG-8120, Rigaku, Tokyo, Japan) were performed up to 200 °C at a heating rate of 20 °C min^{-1} and held at 200 °C for 90 min under airflow.

Results and discussion

The PHEMA and PVA thin-film matrices with 100 nm thickness were prepared by spin-coating and subsequent annealing (Supplementary Fig. S2). After the crystallization process, spherulitic thin-film crystals were observed in the matrices by SEM, and they fully cover the substrates, forming flat thin films (Fig. 2, left and middle). The thickness of the thin-film hybrids was determined by cross-sectional SEM images (Fig. 2, right). The thickness of hybrids consisting of ZHC and PHEMA (ZHC/PHEMA) and ZHC/PVA thin-film hybrids was 250 nm.

Figure 3 shows XRD patterns of the as-prepared thin-film crystals. All the peaks observed in the XRD patterns are assigned to ZHC ($Zn(CO_3)_x(OH)_y{\cdot}nH_2O$; $x = 0.25$, $y = 1.5$, $n = 0.25$ in ICDD no. 011-0287 and $x = 0.4$, $y = 1.2$, $n = 0$ in ICDD no. 019-1458, respectively). The powder sample of the thin-film crystals formed in the PHEMA matrix was collected from the substrate, which also shows a diffraction pattern of ZHC without any distinct orientation (Supplementary Fig. S3).

Preferential crystallographic orientations of ZHC crystals were observed in the XRD patterns of thin-film samples. In the out-of-plane XRD pattern of thin-film samples grown in the PHEMA matrix, the intensified peak of the (200) plane is seen except for the broad peak of the glass substrate at $2\theta = \sim 25°$. In contrast, the in-plane XRD pattern exhibits an intensified peak of the (002) plane of the ZHC crystals.

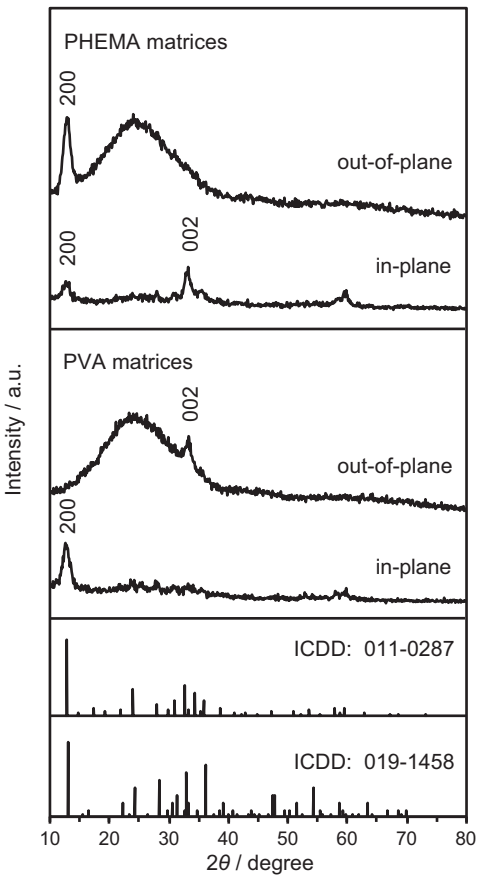

Fig. 3 Out-of-plane and in-plane XRD patterns of the ZHC thin films grown in the PHEMA and PVA matrices after a 24 h crystallization process. The standard powder XRD patterns of a ZHC crystal (ICDD 011-0287 and 019-1458) are shown at the bottom

ZHC crystals grown in the PHEMA matrix were preferentially oriented along the (200) plane parallel to the

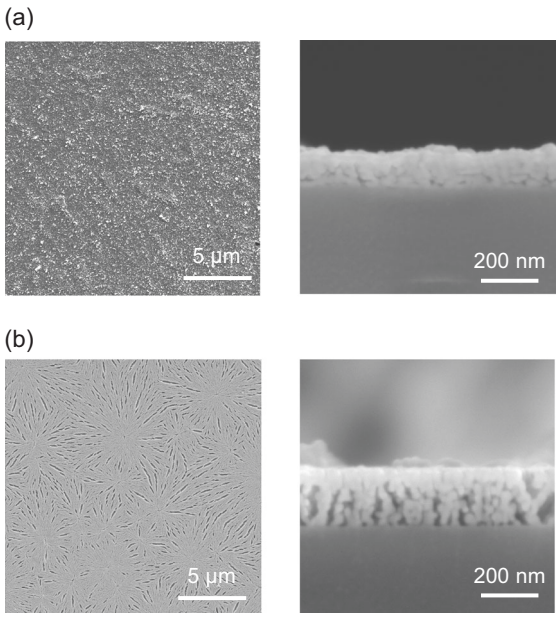

Fig. 4 ZnO thin films through ZHC thin films prepared by using **a** PHEMA and **b** PVA matrices. SEM images of (left) top-view surfaces and (right) cross-sectional SEM images of the thin films

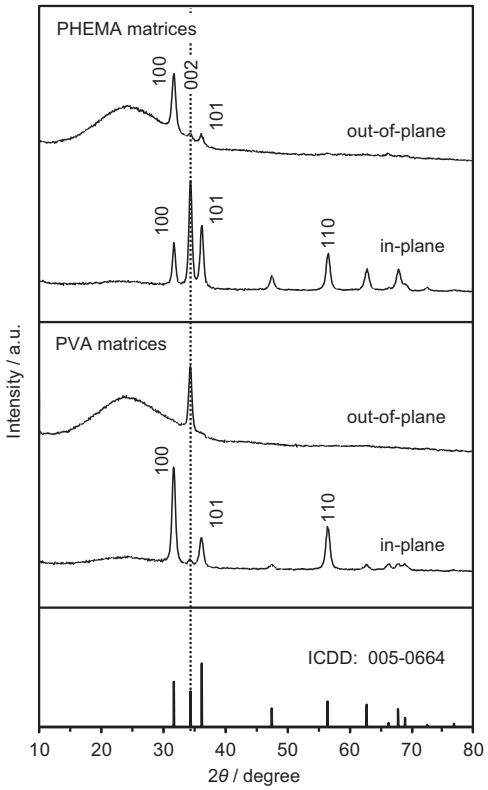

Fig. 5 Out-of-plane and in-plane XRD patterns of the ZnO thin films through ZHC thin films prepared by using PHEMA and PVA matrices. The standard powder XRD pattern of a ZnO crystal (ICDD 005-0664) is shown at the bottom

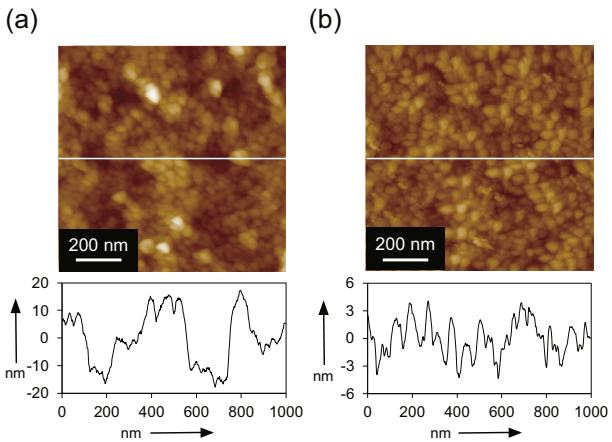

Fig. 6 AFM images of the ZnO thin films prepared by using **a** PHEMA and **b** PVA matrices. (Upper) Top-down view and (lower) cross-sectional view. The white line region shows the measured cross-section

substrate. On the other hand, the thin-film sample grown in the PVA matrix with the same thickness as the PHEMA matrix shows a totally different crystallographic orientation. It exhibits the intensified peak of the (002) plane in the out-of-plane diffraction pattern and the (200) plane in the in-plane diffraction pattern, which suggests that the ZHC crystals are oriented along the (002) plane parallel to the substrate.

In the previous studies on $CaCO_3$ thin film formation, no such drastic change in crystallographic orientation was observed [13–17]. Because ZHC has an anisotropic layered crystal structure [47], the crystal growth direction may easily be affected by the environment. When the bare glass substrate was used in place of the polymer matrix, no crystallization was observed.

These thin-film crystals were converted to ZnO thin films by annealing at 500 °C for 2 h (Fig. 4). Both samples maintained their thin-film morphologies after the thermal treatment. The thickness of the ZnO thin film prepared by using the PHEMA matrix was 150 nm, and that of the ZnO thin film prepared by using the PVA matrix was 200 nm.

XRD patterns of the annealed samples show that ZnO was formed (Fig. 5). The intensities of the (002) peaks are different between the out-of-plane and in-plane XRD patterns. This observation suggests that these ZnO thin films had specific *c*-axis orientations, which were the same as those of the precursor ZHC thin films (Fig. 3). These results indicate that the orientation of ZnO thin films reflects the orientation of ZHC before the conversion. It is noteworthy that the ZnO thin films with the *c*-axis oriented parallel to the substrate were obtained. This orientation is not easy to achieve by widely used methods [40].

The nanostructures of the ZnO thin films were examined with AFM and TEM. The AFM images (Fig. 6) show that the top surface of both samples had a homogeneous distribution of nanocrystals. The TEM observation was carried

out on the samples after scraping the surface of the thin films. The TEM images (Fig. 7) show that both samples were composed of granular crystals with sizes of 10–50 nm, and all the polymer matrices were apparently decomposed.

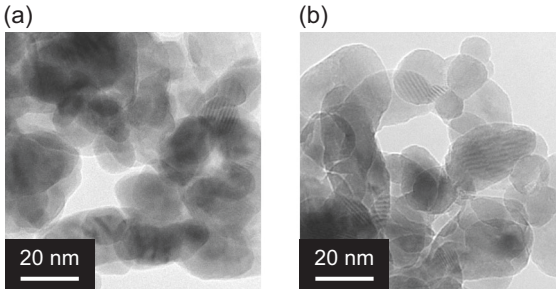

Fig. 7 TEM images of the crystals separated from ZnO thin films prepared by using **a** PHEMA and **b** PVA matrices

To examine the relationship between the polymer matrices and oriented crystallization behavior, the effects of the thickness and annealing time for the matrices on the crystal orientation were studied. The PHEMA and PVA matrices with 100, 300, and 1000 nm thickness annealed at 200 °C for 10, 30, and 90 min (Supplementary Figs. S4 and S5) were used for ZHC crystallization for 24 h. Figure 8 shows the out-of-plane XRD patterns of the as-prepared ZHC thin films. The orientation of ZHC crystals grown in PHEMA matrices is strongly dependent on the thickness and annealing time. The PHEMA matrices with 100 nm thickness annealed for 10 min induce the ZHC crystals to align along the (200) plane parallel to the substrate. In contrast, the peak attributed to the (002) plane of ZHC was observed for the PHEMA matrices with a thickness of 1000

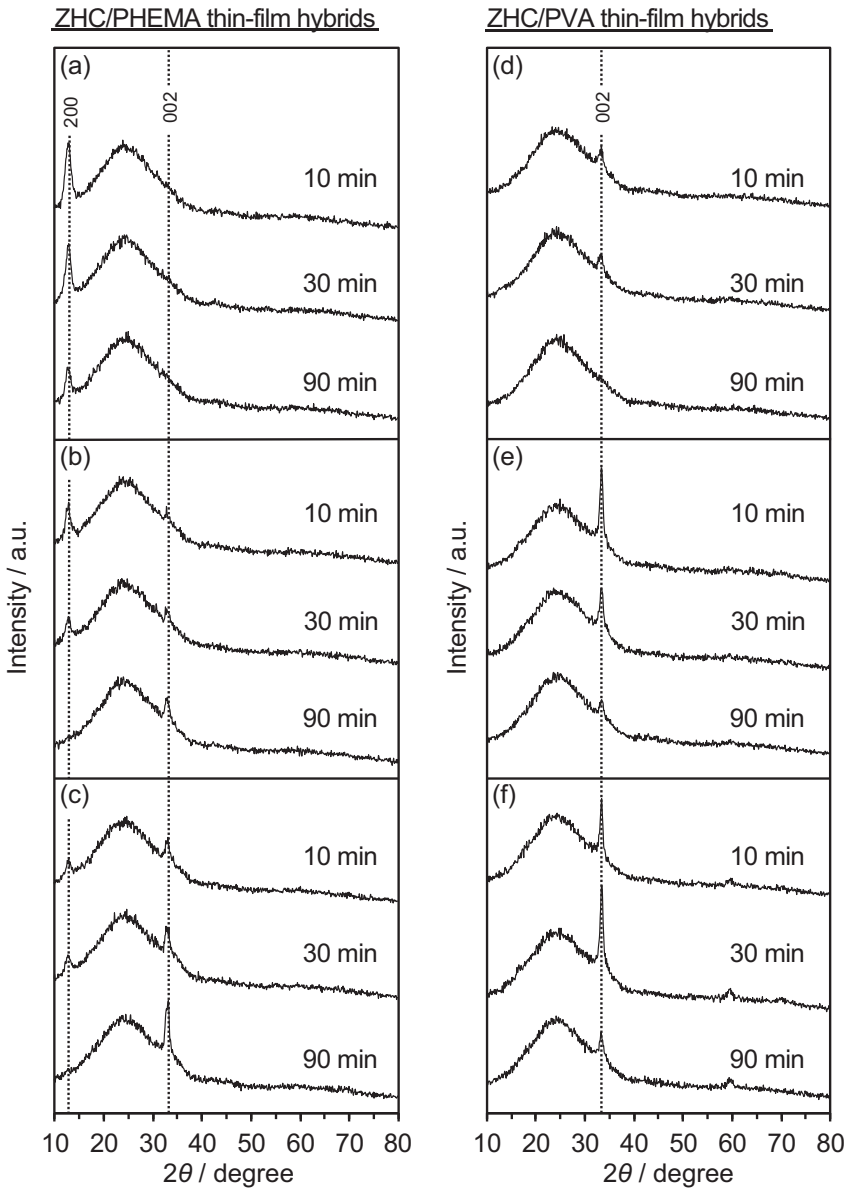

Fig. 8 Out-of-plane XRD patterns of the ZHC thin films prepared by using **a**–**c** PHEMA and **d**–**f** PVA matrices with **a**, **d** 100 nm, **b**, **e** 300 nm, and **c**, **f** 1000 nm thickness annealed at 200 °C for 10, 30, and 90 min

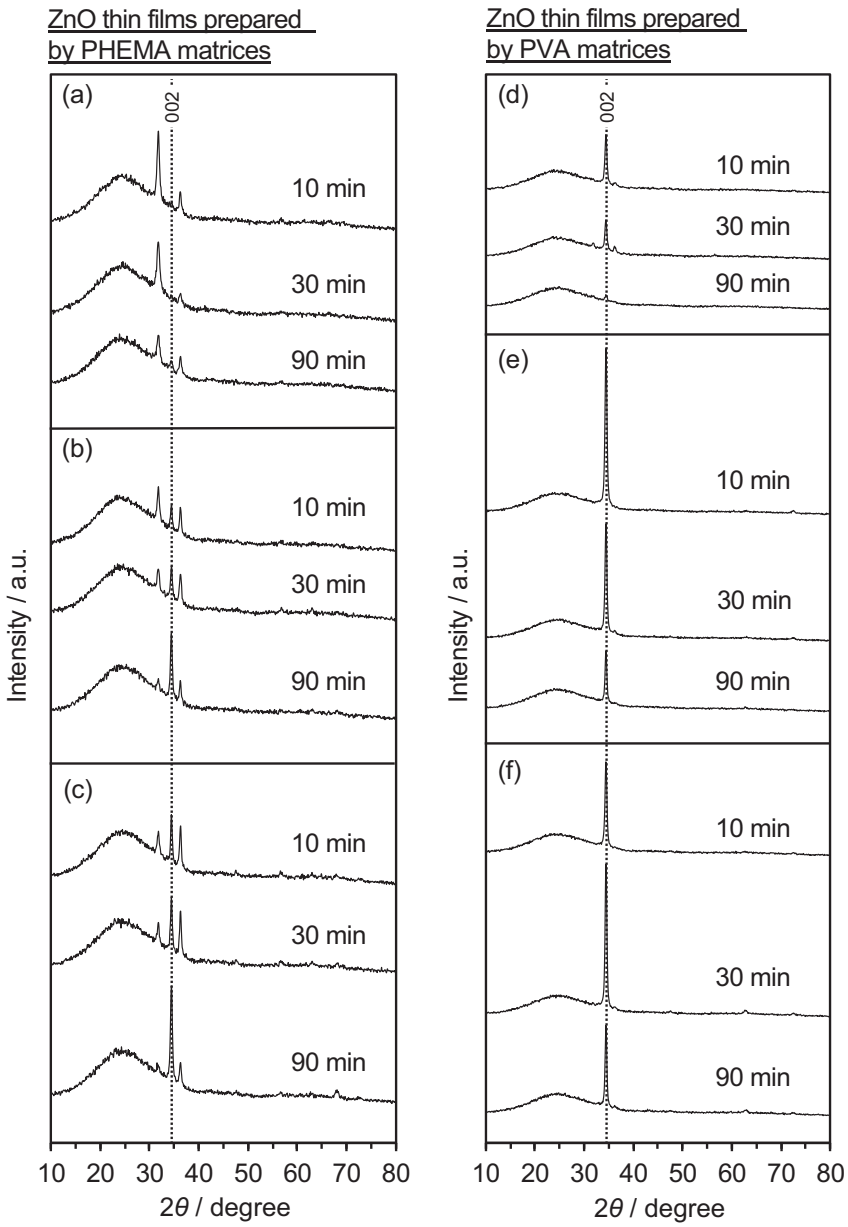

Fig. 9 Out-of-plane XRD patterns of the ZnO thin films prepared by using **a**–**c** PHEMA and **d**–**f** PVA matrices with **a**, **d** 100 nm, **b**, **e** 300 nm, and **c**, **f** 1000 nm thickness annealed at 200 °C for 10, 30, and 90 min

nm that were annealed for 90 min. For the PVA matrices, the ZHC crystals were oriented along the (002) plane parallel to the substrate, and this orientation was not affected by the thickness and annealing time.

The ZHC thin films grown in polymer matrices were converted to ZnO thin films by annealing at 500 °C for 2 h. Figure 9 shows the out-of-plane XRD patterns of ZnO thin films. These results show that the *c*-axis orientation of the resultant ZnO crystals prepared by PHEMA matrices strongly depends on the thickness and annealing time of the matrices. The ZnO thin films prepared by PHEMA matrices with a thickness of 1000 nm and 90 min annealing indicated an intensified peak of the (002) plane. As the thickness and annealing time for the PHEMA matrices decreased, the intensities of the (002) peak decreased. Using PHEMA matrices with 100 nm thickness and 10 min annealing, the (002) peak disappeared, which suggests that the *c*-axis is oriented parallel to the substrate. In contrast, PVA matrices induce the *c*-axis of ZnO crystals to align perpendicular to the substrate almost independently of the thickness and annealing time.

It was reported that the alignment of the plate-like crystals of ZHC depends on the hydrophilicity of the substrate [46]. Taking these results into account, we hypothesized that the hydrophilic environment inside the PHEMA matrices was changed by thermal treatment, while the environment inside the PVA matrices was not changed. In addition to the effects of thermal treatment, the matrix

thickness also affects the hydrophilic environment inside the matrix. It is assumed that the effects of thickness for PHEMA matrices on the hydrophilicity were more significant than those of PVA because the PHEMA matrices were more hydrophobic than the PVA matrices. The PHEMA matrices in the vicinity of the water-matrix interface were highly swollen, while the other part of the thicker matrices tended to be relatively more hydrophobic. Therefore, for PHEMA matrices, the hydrophobic part might increase in proportion to the matrix thickness.

Conclusions

In summary, we have achieved control of the crystallographic orientation of ZnO thin films based on ZHC thin-film hybrids prepared by the biomimetic macromolecular template approach. The PHEMA and PVA matrices largely affected the *c*-axis orientation of the ZHC thin films. It is noteworthy that ZHC and ZnO thin films prepared by using the PHEMA matrix exhibited drastic changes in the *c*-axis orientation depending on the thickness and annealing time of the matrices. We demonstrate that not only the preparation of ZnO thin films but also the tuning of the orientation is possible in a wide range with the combination of the biomimetic macromolecular template approach and thermal treatment. We assume that this method is promising for the future development of new ZnO materials with controlled structures. It is also important that biomimetic syntheses of organic/inorganic hybrids are promising for a sustainable society [48–50].

Acknowledgements This study was partially supported by KAKENHI JP19H05714 and KAKENHI JP19H05715 (Grant-in-Aid for Scientific Research on Innovative Areas of Aquatic Functional Materials, No. 6104) and KAKENHI JP22107003 (Grant-in-Aid for Scientific Research on Innovative Areas of Fusion Materials, No. 2206). The authors also thank the Nanotechnology Platform project of The University of Tokyo for the SEM and TEM observation (Grant No. JPMXP09A21UT0151). TM thanks the World-leading Innovative Graduate Study Program for Materials Research, Information, and Technology (MERIT-WINGS).

Compliance with ethical standards

Conflict of interest The authors declare no competing interests.

Publisher's note Springer Nature remains neutral with regard to jurisdictional claims in published maps and institutional affiliations.

References

1. Mann S. Biomineralization: principles and concepts in bioinorganic materials chemistry. New York: Oxford University Press; 2001.
2. Addadi L, Weiner S. Control and design principles in biological mineralization. Angew Chem Int Ed Engl. 1992;31:153–69.
3. Arakaki A, Shimizu K, Oda M, Sakamoto T, Nishimura T, Kato T. Biomineralization-inspired synthesis of functional organic/inorganic hybrid materials: organic molecular control of self-organization of hybrids. Org Biomol Chem. 2015;13:974–89.
4. Nudelman F, Sommerdijk NAJM. Biomineralization as an inspiration for materials chemistry. Angew Chem Int Ed. 2012;51:6582–96.
5. Yao H-B, Ge J, Mao L-B, Yan Y-X, Yu S-H. 25th anniversary article: artificial carbonate nanocrystals and layered structural nanocomposites inspired by nacre: synthesis, fabrication and applications. Adv Mater. 2014;26:163–88.
6. Cantaert B, Kuo D, Matsumura S, Nishimura T, Sakamoto T, Kato T. Use of amorphous calcium carbonate for the design of new materials. ChemPlusChem. 2017;82:107–20.
7. Du H, Steiner U, Amstad E. Nacre-inspired hard and tough materials. Chimia. 2019;73:29–34.
8. Chen Y, Feng Y, Deveaux JG, Masoud MA, Chandra FS, Chen H, et al. Biomineralization forming process and bio-inspired nanomaterials for biomedical application: a review. Minerals. 2019;9:68.
9. Nishi M, Kobayashi H, Amano T, Sakate Y, Bito T, Arima J, et al. Identification of the domains involved in promotion of silica formation in glassin, a protein occluded in hexactinellid sponge biosilica, for development of a tag for purification and immobilization of recombinant proteins. Mar Biotechnol. 2020;22:739–47.
10. Suzuki M, Saruwatari K, Kogure T, Yamamoto Y, Nishimura T, Kato T, et al. An acidic matrix protein, Pif, is a key macromolecule for nacre formation. Science. 2009;325:1388–90.
11. Metzler RA, Evans JS, Killian CE, Zhou D, Churchill TH, Appathurai NP, et al. Nacre protein fragment templates lamellar aragonite growth. J Am Chem Soc. 2010;132:6329–34.
12. Siponen MI, Legrand P, Widdrat M, Jones SR, Zhang W-J, Chang MCY, et al. Structural insight into magnetochrome-mediated magnetite biomineralization. Nature. 2013;502:681–4.
13. Kato T, Suzuki T, Irie T. Layered thin-film composite consisting of polymers and calcium carbonate: a novel organic/inorganic material with an organized structure. Chem Lett. 2000;29:186–7.
14. Hosoda N, Kato T. Thin-film formation of calcium carbonate crystals: effects of functional groups of matrix polymers. Chem Mater. 2001;13:688–93.
15. Katsumura A, Sugimura K, Nishio Y. Calcium carbonate mineralization in chiral mesomorphic order-retaining ethyl cellulose/poly(acrylic acid) composite films. Polymer. 2018;139:26–35.
16. Hosoda N, Sugawara A, Kato T. Template effect of crystalline poly(vinyl alcohol) for selective formation of aragonite and vaterite $CaCO_3$ thin films. Macromolecules. 2003;36:6449–52.
17. Sakamoto T, Oichi A, Oaki Y, Nishimura T, Sugawara A, Kato T. Three-dimensional relief structures of $CaCO_3$ crystal assemblies formed by spontaneous two-step crystal growth on a polymer thin film. Cryst Growth Des. 2009;9:622–5.
18. Kajiyama S, Sakamoto T, Inoue M, Nishimura T, Yokoi T, Ohtsuki C, et al. Rapid and topotactic transformation from

octacalcium phosphate to hydroxyapatite (HAP): A new approach to self-organization of free-standing thin-film HAP-based nanohybrids. CrystEngComm. 2016;18:8388–95.
19. Xiao C, Li M, Wang B, Liu M-F, Shao C, Pan H, et al. Total morphosynthesis of biomimetic prismatic-type $CaCO_3$ thin films. Nat Commun. 2017;8:1398.
20. Wang B, Mao L-B, Li M, Chen Y, Liu M-F, Xiao C, et al. Synergistic effect of granular seed substrates and soluble additives in structural control of prismatic $CaCO_3$ thin films. Langmuir. 2018;34:11126–38.
21. Ichikawa R, Kajiyama S, Iimura M, Kato T. Tuning the *c*-axis orientation of calcium phosphate hybrid thin films using polymer templates. Langmuir. 2019;35:4077–84.
22. Han Y, Nishimura T, Iimura M, Sakamoto T, Ohtsuki C, Kato T. Periodic surface-ring pattern formation for hydroxyapatite thin films formed by biomineralization-inspired processes. Langmuir. 2017;33:10077–83.
23. Han Y, Nishimura T, Kato T. Morphology tuning in the formation of vaterite crystal thin films with thermoresponsive poly(*N*-isopropylacrylamide) brush matrices. CrystEngComm. 2014;16:3540–7.
24. Sugawara A, Nishimura T, Yamamoto Y, Inoue H, Nagasawa H, Kato T. Self-organization of oriented calcium carbonate/polymer composites: effects of a matrix peptide isolated from the exoskeleton of a crayfish. Angew Chem Int Ed. 2006;45:2876–9.
25. Kumagai H, Matsunaga R, Nishimura T, Yamamoto Y, Kajiyama S, Oaki Y, et al. $CaCO_3$/chitin hybrids: recombinant acidic peptides based on a peptide extracted from the exoskeleton of a crayfish controls the structures of the hybrids. Faraday Discuss. 2012;159:483.
26. Addadi L, Raz S, Weiner S. Taking advantage of disorder: amorphous calcium carbonate and its roles in biomineralization. Adv Mater. 2003;15:959–70.
27. Gower LB. Biomimetic model systems for investigating the amorphous precursor pathway and its role in biomineralization. Chem Rev. 2008;108:4551–627.
28. Oaki Y, Kajiyama S, Nishimura T, Imai H, Kato T. Nanosegregated amorphous composites of calcium carbonate and an organic polymer. Adv Mater. 2008;20:3633–7.
29. Kajiyama S, Nishimura T, Sakamoto T, Kato T. Aragonite nanorods in calcium carbonate/polymer hybrids formed through self-organization processes from amorphous calcium carbonate solution. Small. 2014;10:1634–41.
30. Saito T, Oaki Y, Nishimura T, Isogai A, Kato T. Bioinspired stiff and flexible composites of nanocellulose-reinforced amorphous $CaCO_3$. Mater Horiz. 2014;1:321–5.
31. Sun S, Mao L-B, Lei Z, Yu S-H, Cölfen H. Hydrogels from amorphous calcium carbonate and polyacrylic acid: bio-inspired materials for "mineral plastics". Angew Chem Int Ed. 2016;55:11765–9.
32. Gebauer D, Oliynyk V, Salajkova M, Sort J, Zhou Q, Bergström L, et al. A transparent hybrid of nanocrystalline cellulose and amorphous calcium carbonate nanoparticles. Nanoscale. 2011;3:3563–6.
33. Zhu F, Nishimura T, Kato T. Organic/inorganic fusion materials: cyclodextrin-based polymer/$CaCO_3$ hybrids incorporating dye molecules through host–guest interactions. Polym J. 2015;47:122–7.
34. Matsumura S, Kajiyama S, Nishimura T, Kato T. Formation of helically structured chitin/$CaCO_3$ hybrids through an approach inspired by the biomineralization processes of crustacean cuticles. Small. 2015;11:5127–33.
35. Umetsu M, Mizuta M, Tsumoto K, Ohara S, Takami S, Watanabe H, et al. Bioassisted room-temperature immobilization and mineralization of zinc oxide—the structural ordering of ZnO nanoparticles into a flower-type morphology. Adv Mater. 2005;17:2571–5.
36. Zhang Y, Yang H, Zhang G, Cui J, Zhan J. The fabrication of oriented ZnO porous nanoplates on the silver foil with tunable hydrophobicity. CrystEngComm. 2014;16:1831.
37. Wang L, Li X, Li Q, Yu X, Zhao Y, Zhang J, et al. Oriented polarization tuning broadband absorption from flexible hierarchical ZnO arrays vertically supported on carbon cloth. Small. 2019;15:1900900.
38. Lou C, Wang K, Mei H, Xie J, Zheng W, Liu X, et al. ZnO nanoarrays via a thermal decomposition–deposition method for sensitive and selective NO_2 detection. CrystEngComm. 2021;23:3654–63.
39. Park BC, Byun SW, Ju Y, Lee DB, Shin JB, Yeon K, et al. Zinc oxide nano-spicules on polylactic acid for super-hydrophilic and bactericidal surfaces. Adv Funct Mater. 2021;31:2100844.
40. Yan R, Takahashi T, Zeng H, Hosomi T, Kanai M, Zhang G, et al. Robust and electrically conductive ZnO thin films and nanostructures: their applications in thermally and chemically harsh environments. ACS Appl Electron Mater. 2021;3:2925–40.
41. Matsumura S, Horiguchi Y, Nishimura T, Sakai H, Kato T. Biomineralization-inspired preparation of zinc hydroxide carbonate/polymer hybrids and their conversion into zinc oxide thin-film photocatalysts. Chem Eur J. 2016;22:7094–101.
42. Kuo D, Kajiyama S, Kato T. Development of biomineralization-inspired hybrids based on β-chitin and zinc hydroxide carbonate and their conversion into zinc oxide thin films. CrystEngComm. 2019;21:2893–9.
43. Katase F, Kajiyama S, Kato T. Macromolecular templates for biomineralization-inspired crystallization of oriented layered zinc hydroxides. Polym J. 2017;49:735–9.
44. Yanagitani T, Matsukawa M, Watanabe Y, Otani T. Formation of uniaxially (11$\bar{2}$0) textured ZnO films on glass substrates. J Cryst Growth. 2005;276:424–30.
45. Morita T, Ueno S, Hosono E, Zhou H, Hagiwara M, Fujihara S. Fabrication of transparent conductive zinc oxide films by chemical bath deposition using solutions containing Zn^{2+} and Al^{3+} ions. J Ceram Soc Jpn. 2015;123:329–34.
46. Hosono E, Fujihara S, Honma I, Zhou H. The fabrication of an upright-standing zinc oxide nanosheet for use in dye-sensitized solar cells. Adv Mater. 2005;17:2091–4.
47. Ghose S. The crystal structure of hydrozincite, $Zn_5(OH)_6(CO_3)_2$. Acta Cryst. 1964;17:1051–7.
48. Yamada M, Tsuruzumi M. Utilization of milk protein as an environmental material: accumulation of metal ions using a protein–inorganic hybrid material. Polym J. 2016;48:295–300.
49. Zhou H, Wang Y, Lu H. Intracellular delivery of His-tagged proteins via a hybrid organic–inorganic nanoparticle. Polym J. 2021;53:1259–67.
50. Wegst UGK, Bai H, Saiz E, Tomsia AP, Ritchie RO. Bioinspired structural materials. Nat Mater. 2015;14:23–36.